Available online at www.sciencedirect.com
ScienceDirect
Trans. Nonferrous Met. Soc. China 31(2021) 2861−2870
Transactions of Nonferrous Metals Society of China
www.tnmsc.cn

Composition and structure of arsenic−antimony alloy electrodeposited from acidic chloride solution

Yan-xiang SHU, Hua-zhen CAO, Hui-bin ZHANG, Sheng-hang XU, Guang-ya HOU, Yi-ping TANG, Guo-qu ZHENG

College of Materials Science and Engineering, Zhejiang University of Technology, Hangzhou 310014, China

Received 29 October 2020; accepted 18 June 2021

Abstract: AsSb alloy (0.70−95.81 wt.% As) was prepared by electrodeposition in As(III) and Sb(III) contained electrolytes. The influence of electrolyte composition, hydrochloric acid concentration, and temperature on the composition and structure of AsSb deposits was studied. The electroreduction mechanism of As(III) and Sb(III) in hydrochloric acid solution was revealed via thermodynamic analysis. The results show that the increase of H^+ concentration promotes the reduction of As(III), while the increase of Cl^- concentration significantly inhibits the reduction of Sb(III). As a result, the As content in deposits increases gradually with the increase of hydrochloric acid concentration. Simultaneously, the phase structure of AsSb deposits evolves from crystalline to amorphous. When the As content is 24.55−33.75 wt.%, AsSb mixed crystal is obtained. The electrolysis temperature has little effect on the deposits composition, but the structure of deposits evolves from crystalline to amorphous with decreasing the temperature.

Key words: AsSb alloy; composition; phase structure; hydrochloric acid; thermodynamic analysis

1 Introduction

Arsenic is a dangerous pollutant [1,2] but an important resource. The traditional treatment methods of arsenic in waste water include precipitation [3−5], adsorption [6], membrane separation [7], ion exchange [8], oxidation [9], etc. The arsenic-containing waste produced by these disposal methods is likely to cause secondary pollution [10]. A promising technology for arsenic-containing solution treatment should be comprehensive recovery, i.e. eliminating the arsenic contamination and at the same time producing valuable arsenic products. Therefore, the application of electrochemical technology to recover elemental arsenic from high-concentration arsenic wastewater seems to be an attractive way [11]. However, there are many limitations, such as the inevitably released arsine gas with high toxicity during the electrodeposition process [12,13] and the self-inhibition phenomenon caused by the non-conductivity of elemental arsenic. In our previous studies [14,15], we found that the addition of ammonium citrate [16] or Sb(III) ions [17] could inhibit the produce of arsine effectively, and AsSb alloy was obtained by continuous electrodeposition in arsenic-containing hydrochloric acid solution derived from the treatment of lead anode slime [18].

In addition, As_xSb_{1-x} [19], $GaAs_xSb_{1-x}$ [20], $AlGaAs_{0.1}Sb_{0.9}$ [21], $InGaAs_{0.75}Sb_{0.25}$ [22] and other arsenic-containing alloys [23] have broad potential applications in the fields of photovoltaic [24], semiconductor [25], thermoelectric [26] and thermomagnetic [27] materials. At present, the main preparation methods of AsSb alloy and III-AsSb alloy are metal organic vapor phase epitaxy (MOVPE) and molecular beam epitaxy (MBE). However, these methods have many disadvantages, such as toxicity of raw materials,

Corresponding author: Guo-qu ZHENG, E-mail: zgq003047@163.com; Hua-zhen CAO, E-mail: caohz@zjut.edu.cn
DOI: 10.1016/S1003-6326(21)65699-6

high cost, and low efficiency. At this point, electrochemical deposition method is a promising candidate in both academic and industrial aspects.

As we know, the composition and structure of alloys are of great importance for the application. The crystal structures depend strongly on the alloy composition, and the composition is usually affected by electrolyte components and electrolytic parameters. In this work, we found that hydrochloric acid has a special influence on the composition of AsSb electrodeposits. So far, there has been less relevant researches on this issue. To reveal the underlying mechanism of hydrochloric acid on arsenic and antimony reduction, we systemically investigate the electrochemical behaviours of As(III) and Sb(III) with different H^+ and Cl^- concentrations via thermodynamic analysis. Moreover, crystal structure evolution of AsSb electrodeposits was also investigated detailedly. This study provides a novel way to control the composition and phase structure of AsSb alloy directly by electrodeposition process, opening a new path for preparation of alloy with different purposes.

2 Experimental

2.1 Materials

The electrolytes were prepared with acidic $AsCl_3$ aqueous solution (derived from the chloridizing−leaching process of lead anode slime) and $SbCl_3$ (AR, 99%). H^+ and Cl^- concentrations were adjusted by adding HCl and NaCl.

2.2 Electrochemical measurements

Linear sweep voltammetry (LSV) curves were measured on a CHI660 electrochemical workstation (CHI Instruments, Shanghai, China) using glassy carbon electrode (GCE, exposed area of 7.065 mm^2) as working electrode, platinum plate (exposed area of 4.5 cm^2) as counter electrode and saturated calomel electrode (SCE) as reference electrode. The potential was swept negatively from open circuit potential to −0.8 V at a scanning rate of 50 mV/s. All tests were carried out at 30 °C.

2.3 Electrodeposition experiments

AsSb alloy electrodeposition was performed in galvanostatic regime (4 mA/cm^2) for 1 h using copper as cathode and platinum as anode, which were placed face to face with a distance of 70 mm. All experiments were carried out at 10−40 °C.

2.4 Characterization

The phase structure of deposits was characterized by X-ray diffraction technique (XRD, RIGAKU D/Max 2550 PC). The composition of deposits was determined by energy dispersive X-ray fluorescence spectroscopy (EDX-LE). The morphology of the deposit was observed by scanning electron microscopy (SEM, FEI nano nova 450).

2.5 Thermodynamic calculation

The φ−pH diagram and φ−lg[Cl^-] diagram of As(III)−Sb(III)−HCl system were made based on the thermodynamic data shown in Table 1 [28,29], for the purpose of analyzing the main species and their redox equilibrium potentials.

3 Results and discussion

3.1 Effects of hydrochloric acid on AsSb electrodeposition

The electrodeposition characteristic of AsSb

Table 1 Reactions and its φ−pH/φ−lg[Cl^-] equations in As(III)−Sb(III)−HCl system at 25 °C

No.	Reaction	φ^0/V	Equation
1	$H_3AsO_3+3H^++3e=As+3H_2O$	0.240	$\varphi=0.240+0.0197\lg[H_3AsO_3]-0.0591pH$
2	$As(OH)_2Cl+2H^++3e=As+2H_2O+Cl^-$	0.261	$\varphi=0.261+0.0197\lg[As(OH)_2Cl]-0.0197\lg[Cl^-]-0.0394pH$
3	$As(OH)Cl_2+H^++3e=As+H_2O+2Cl^-$	0.330	$\varphi=0.330+0.0197\lg[As(OH)Cl_2]-0.0394\lg[Cl^-]-0.0197pH$
4	$AsCl_3+3e=As+3Cl^-$	0.412	$\varphi=0.412+0.0197\lg[AsCl_3]-0.0591\lg[Cl^-]$
5	$2H^++2e=H_2$	0	$\varphi=-0.0591pH$
6	$SbCl_4^-+3e=Sb+4Cl^-$	0.014	$\varphi=0.014+0.0197\lg[SbCl_4^-]-0.0789\lg[Cl^-]$
7	$SbCl_5^{2-}+3e=Sb+5Cl^-$	0.015	$\varphi=0.015+0.0197\lg[SbCl_5^{2-}]-0.0986\lg[Cl^-]$
8	$SbCl_6^{3-}+3e=Sb+6Cl^-$	0.026	$\varphi=0.026+0.0197\lg[SbCl_6^{3-}]-0.1183\lg[Cl^-]$

alloy in low arsenic and high antimony electrolyte (0.2 g/L As(III) and 9.8 g/L Sb(III)) was first investigated. As shown in Fig. 1(a), the As/Sb ratio in deposits increases gradually with increasing the concentration of HCl. It can be seen that the content of As in deposits increases from 0.70 to 35.86 wt.% when the HCl concentration is increased from 2.0 to 5.0 mol/L. In addition, the As content in deposits also depends on the As(III) concentration in electrolyte, as shown in Fig. 1(b). In the electrolyte with 5.0 g/L of As(III) and 1.0 g/L Sb(III), the As content in deposits reaches up to 95.81 wt.% at HCl concentration of 5.0 mol/L.

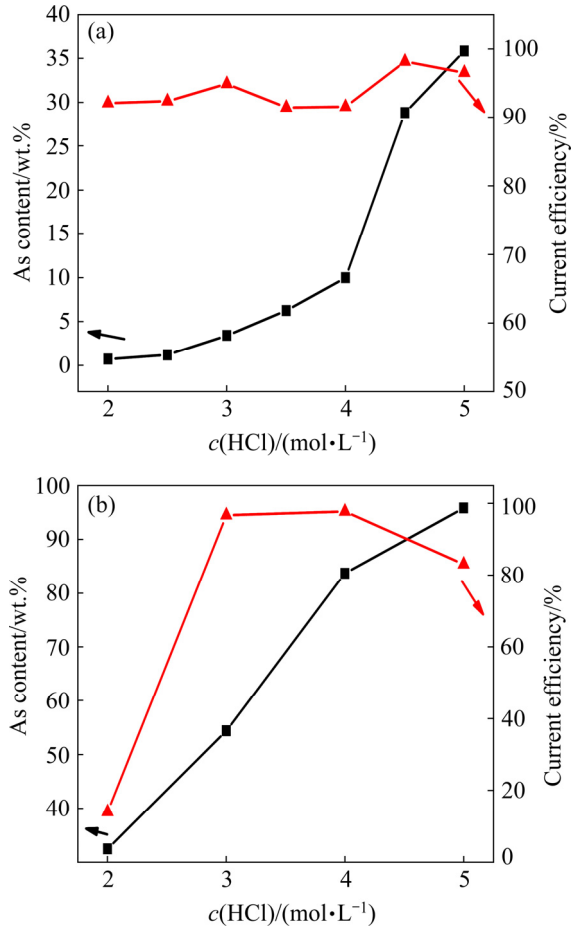

Fig. 1 As content in deposits and current efficiency under different conditions: (a) 0.2 g/L As(III) and 9.8 g/L Sb(III); (b) 5.0 g/L As(III) and 1.0 g/L Sb(III)

In low arsenic-containing solutions, the current efficiency is maintained above 90%. In high arsenic-containing solutions, the current efficiency tends to decrease at high HCl concentration, and it is found that low HCl concentration leads to extremely low current efficiency, which may be related to the incompact structure of deposits in this case.

Figure 2 shows the XRD patterns of electrodeposits prepared from the above-mentioned solutions with different HCl concentrations. It can be seen that the deposits prepared at low HCl concentrations are crystallines, and in other words, low As deposits show a crystalline structure, as indicated by the sharp diffraction peaks on the XRD patterns. With the increasing of HCl concentration, the As content in deposits increases, which finally leads to an amorphous structure.

Figure 2(a) shows the XRD patterns of deposits from electrolyte with low As(III) concentration. According to the Joint Committee on Powder Diffraction Standards (01-071-1173), the diffraction peaks appearing at about 2θ=28.72°, 40.08°, 42.04°, 51.73°, 59.46°, 66.01°, 68.85°, 75.55° and 76.94° are attributed to Sb. There is no peak related to pristine As, which may be ascribed to the fact that the As atoms enter into the crystal lattice of antimony in the form of solid solution, then forming an AsSb alloy instead of an intermetallic compound. From the partially magnified images in Part 1 and Part 2, it can be found that as the concentration of HCl increases, the diffraction peaks of Sb(012), (104), (110) are slightly shifted to the right. The above analysis indicates that the addition of HCl will lead to the rise of arsenic content in deposits, from which we can speculate that it may be also the main reason causing the shift of Sb diffraction peaks. As we know that the As atom radius is smaller than the Sb atom radius, when the As atom takes the place of Sb atom in the lattice, the interplanar distance of Sb will decrease and then the diffraction angle increases accordingly. For the deposits from electrolytes with high As(III) concentration (Fig. 2(b)), two distinct broad peaks in 2θ range of 20°−40° and 45°−60° are observed when the HCl concentration is higher than 3.0 mol/L, indicating that the deposits present an amorphous structure in these conditions.

Figure 3 displays the SEM images of deposits prepared under different HCl concentrations. It can be clearly seen that some protruding particles grow on the surface, and the particle size increases with the increasing of HCl concentration. When the HCl concentration reaches 3.5 mol/L, the protruding particles change into cubic shape. Lamellar defects

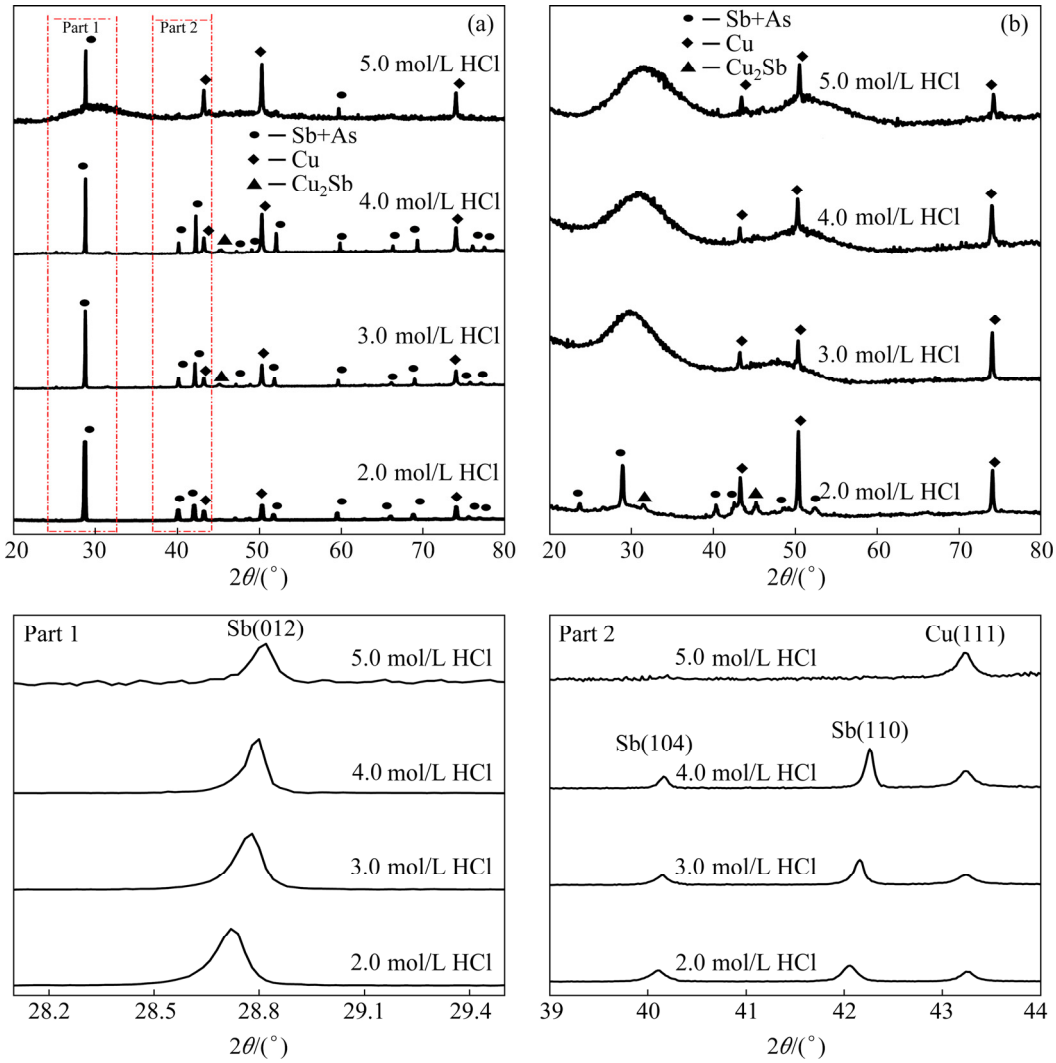

Fig. 2 XRD patterns of electrodeposits prepared from different solutions: (a) 0.2 g/L As(III), 9.8 g/L Sb(III) and different HCl concentrations; (b) 5.0 g/L As(III), 1.0 g/L Sb(III) and different HCl concentrations

are found on the surface of cube particles at HCl concentration of 4.0 mol/L. The excess of hydrochloric acid (i.e. 4.5 mol/L) will cause the particles to transform into wheat spike shape.

These different morphologies and crystal structures are largely attributed to the composition changes in the deposits. In the As(III)−Sb(III)−HCl system, As content in deposits rises with the increase of HCl concentration; that is, As content can be regulated by HCl. Thus, single-variable conditional experiments were designed in order to reveal the effects of H^+ and Cl^- ions in electrodeposition process, respectively.

Herein, the concentrations of As(III), Sb(III) and Cl^- in solutions were kept constant, but H^+ concentration ranged from 2.0 to 5.0 mol/L. As shown in Fig. 4(a), the as-obtained deposits possess a broad range of As content from 9.64 to 35.86 wt.%. The effect of Cl^- on As content in deposits was tested by using solutions with same H^+ concentration while Cl^- concentration from 2.0 to 5.0 mol/L. In this case, the As content varied from 0.70 to 9.64 wt.%. These results indicate that the increasing in H^+ concentration or Cl^- concentration can sharply raise the content of As. It is worth mentioning that the current efficiency is above 90% in all experimental conditions.

Therefore, to reveal the cathodic reaction mechanism, a set of linear sweep voltammetry curves with different H^+ or Cl^- concentrations were measured. In Fig. 5(a), two cathodic peaks are observed at −0.15 V (vs SCE) (P1) and −0.43 V (vs SCE) (P2), which correspond to the reduction of As(III) to elementary arsenic and the evolution of

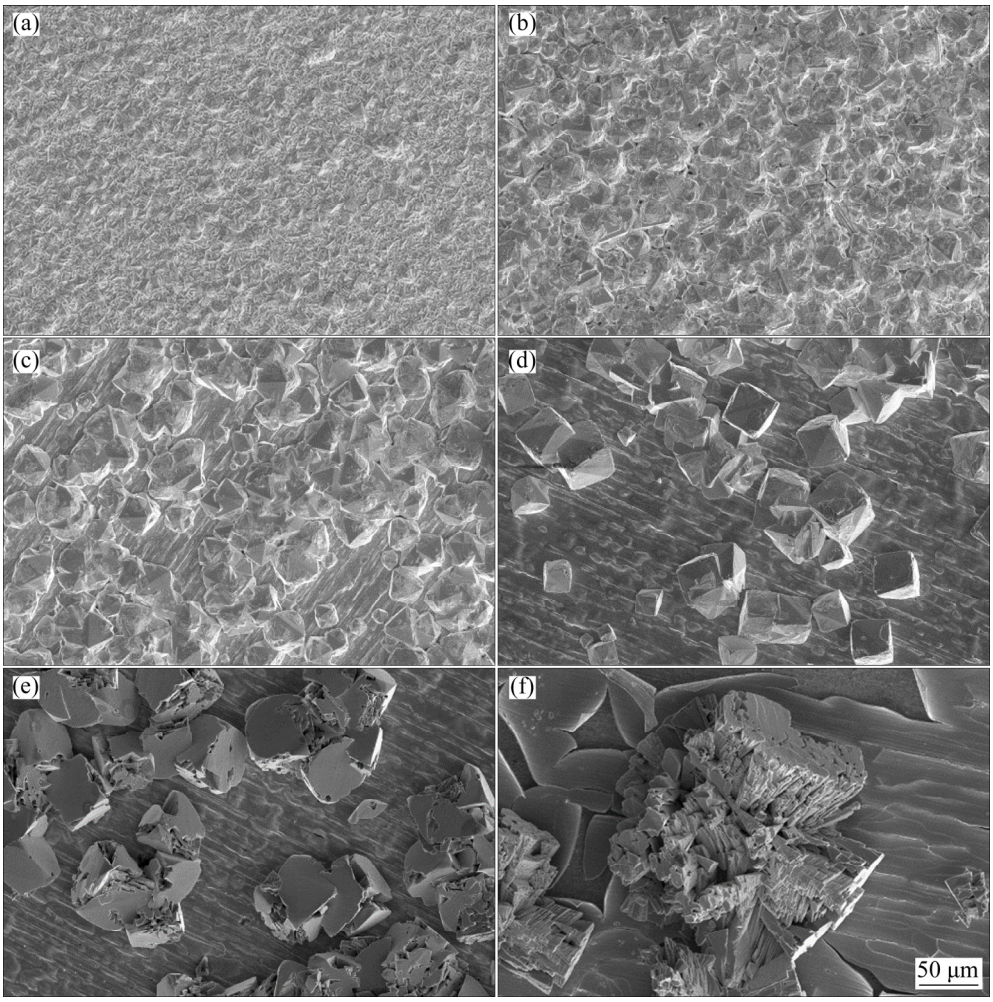

Fig. 3 Morphologies of cathodic deposits obtained from solutions with 0.2 g/L As(III), 9.8 g/L Sb(III) and different HCl concentrations: (a) 2.0 mol/L; (b) 2.5 mol/L; (c) 3.0 mol/L; (d) 3.5 mol/L; (e) 4.0 mol/L; (f) 4.5 mol/L

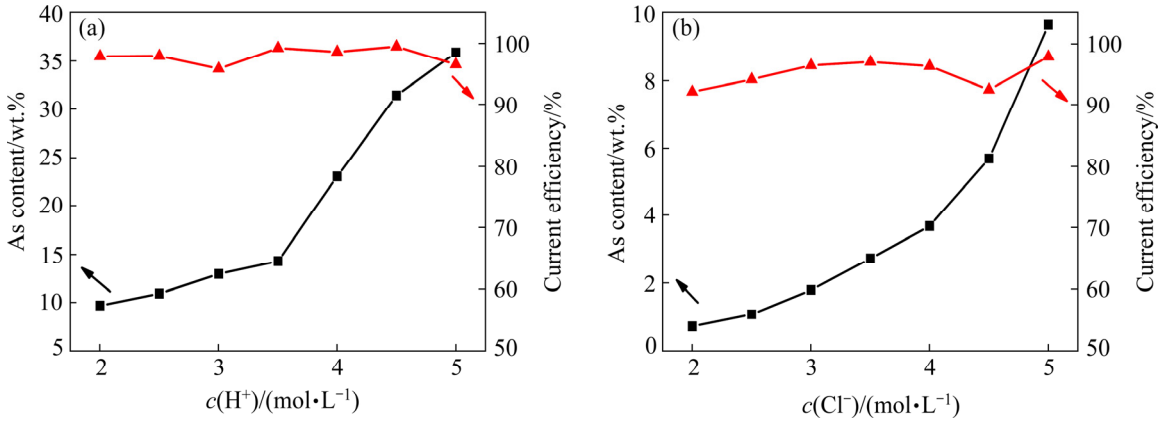

Fig. 4 As content in deposits and current efficiency with different H^+ and Cl^- concentrations (0.2 g/L As(III) and 9.8 g/L Sb(III)): (a) 5.0 mol/L Cl^-; (b) 2.0 mol/L H^+

arsine, respectively. With the increasing of H^+ concentration, the peak current of P1 rises gradually, which indicates that the adding of H^+ is beneficial to the deposition of As. On the contrary, Cl^- concentration has little influence on the reduction of As(III) (Fig. 5(b)) and there is no significant change in the potential range. Figures 5(c, d) represent the effects of Cl^- and H^+ concentrations on the reduction of Sb(III). One strong peak appears from −0.30 to −0.35 V (vs

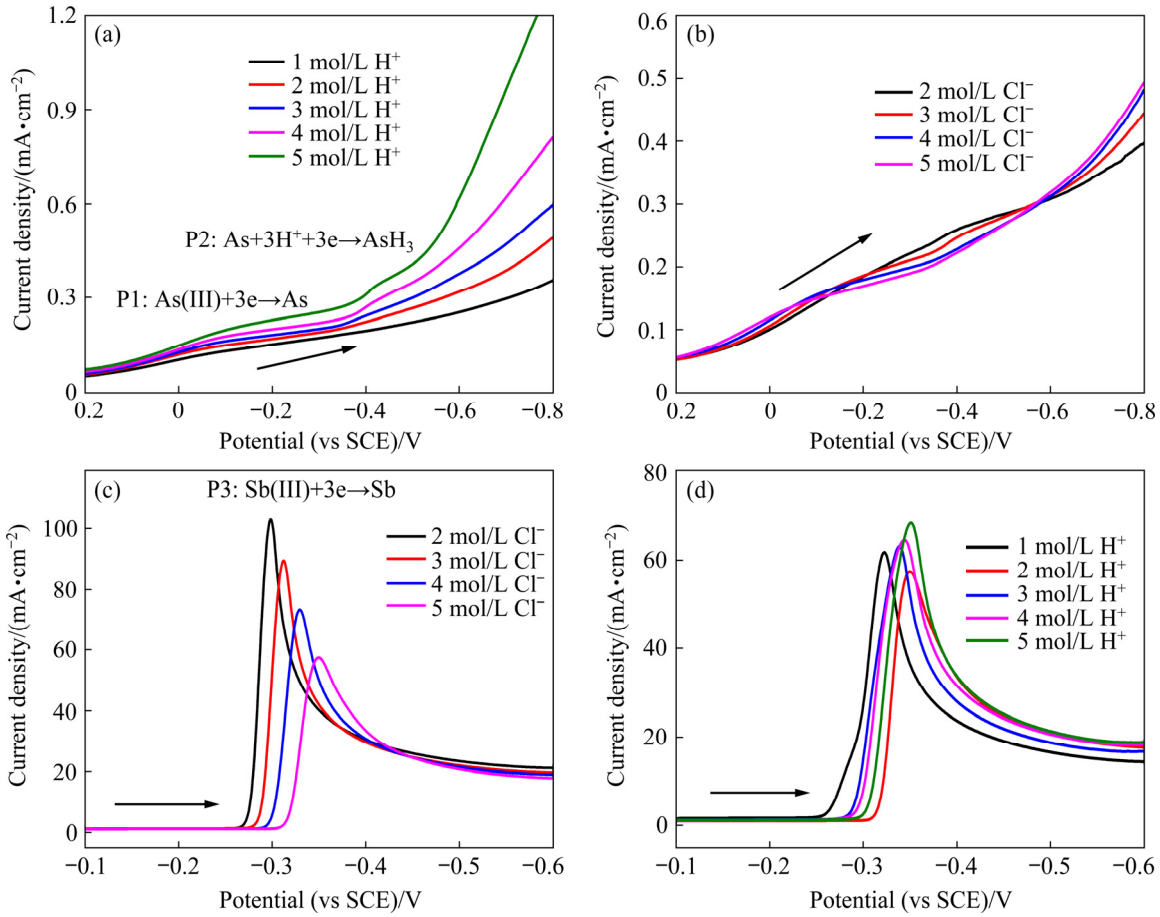

Fig. 5 LSV curves of GCE in different solutions: (a) 0.2 g/L As(III), 5.0 mol/L Cl^-; (b) 0.2 g/L As(III), 2.0 mol/L H^+; (c) 9.8 g/L Sb(III), 2.0 mol/L H^+; (d) 9.8 g/L Sb(III), 5.0 mol/L Cl^-

SCE) (P3), which is ascribed to the reduction of Sb(III) to Sb. It is noted that the Peak P3 shifts negatively with the increasing of Cl^- concentration and the peak current decreases gradually, which indicates that the adding of Cl^- inhibits the reduction of Sb(III). In addition, it is also observed that the H^+ concentration has a slight effect on the reduction of Sb(III). The main reactions in the experimental system are as follows:

$$As(OH)_2Cl+2H^++3e=As+2H_2O+Cl^- \quad (1)$$

$$H_3AsO_3+3H^++3e=As+3H_2O \quad (2)$$

$$SbCl_5^{2-}+3e=Sb+5Cl^- \quad (3)$$

$$SbCl_6^{3-}+3e=Sb+6Cl^- \quad (4)$$

H^+ ions participate in the reduction reaction of arsenic. According to the chemical reaction equilibrium, the adding of H^+ promotes the formation of As. Conversely, the reduction reaction of antimony will produce Cl^-; that is, high Cl^- concentration does not benefit the formation of Sb.

To further elucidate the mechanism, thermodynamic analysis was conducted. Associating the φ_h–pH diagrams (Fig. 6(a)) and the φ_h–lg[Cl^-] diagrams (Fig. 6(b)), we can observe that the main species and their redox equilibrium potentials are changed with H^+ and Cl^- concentrations. In the high-chlorine solution, the main existence form of Sb(III) is $SbCl_6^{3-}$, while As(III) exists in the form of H_3AsO_3 and $As(OH)_2Cl$ when H^+ concentration varies from 2.0 to 5.0 mol/L. With the increase of acidity, the reduction potential of As(III) shifts to the positive direction gradually while the reduction potential of Sb(III) is independent on the acidity. In the high acid solution, the existence forms of Sb(III) are $SbCl_5^{2-}$ and $SbCl_6^{3-}$, and the main species of As(III) is H_3AsO_3 with Cl^- concentration of 2.0−5.0 mol/L. With the increase of Cl^- concentration, the reduction potential of As(III) remains unchanged, while the reduction potential of Sb(III) becomes negative gradually. Based the above thermodynamic analysis, As(III) is likely to be reduced and the reduction of Sb(III) becomes difficult with the adding of HCl, which ultimately

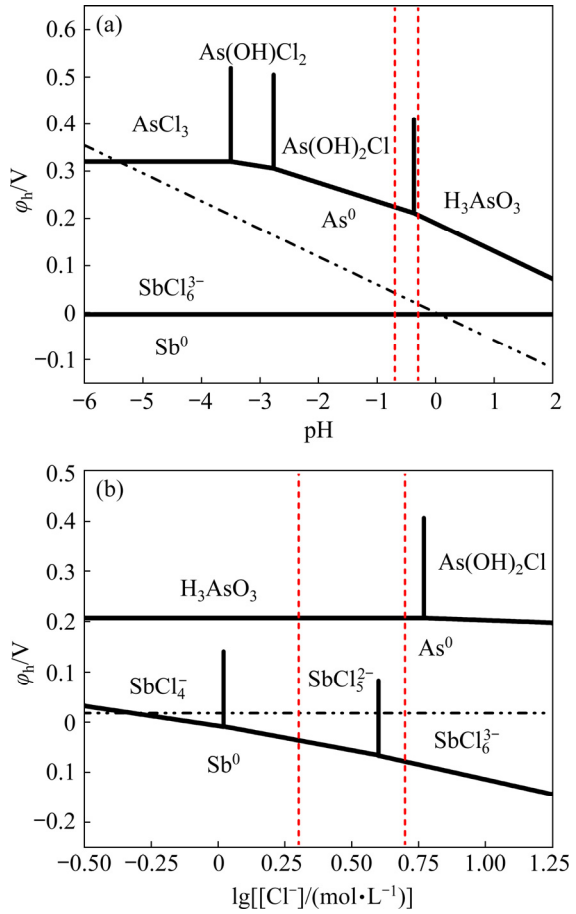

Fig. 6 Calculated φ_h–pH diagrams (a) and φ_h–lg[Cl^-] diagrams (b) of As(III)–Sb(III)–HCl system at 25 °C (0.2 g/L As(III), 9.8 g/L Sb(III)): (a) 5.0 mol/L Cl^-; (b) 2.0 mol/L H^+

results in the significant increase of As content in the deposits.

The effects of HCl concentration on the crystal structure and As content of electrodeposits are shown in Fig. 7. Crystalline deposits with 8.00−9.80 wt.% of As are obtained under low HCl concentrations (2.5−3.0 mol/L). When the HCl concentration reaches 3.5 mol/L, the deposits turn to mixed structure (coexistence of crystalline and amorphous states), which has As content of 24.19 wt.%. In the case of high HCl concentration (4.0−5.0 mol/L), the As content ranges from 46.55 to 76.98 wt.% and the deposits are completely transformed to amorphous structure. That is to say, with the increase of HCl concentration, the As content in deposits increases gradually and the structure evolves from crystalline to amorphous.

3.2 Effects of As(III) and Sb(III) concentrations on AsSb electrodeposition

The composition and crystal structure of deposits prepared under different As(III)/Sb(III) mass ratios were studied by X-diffraction spectra combined with energy dispersive X-ray fluorescence spectroscopy. In this experiment, the total concentration of As(III) and Sb(III) was controlled at about 5.0 g/L. It is clearly seen from Fig. 8 that crystalline-state deposits can be obtained when the electrolyte has a low As(III)/Sb(III) ratio (<0.67), and in this case, the As content in deposits is below 22.58 wt.%. Naturally, the As content in deposits rises with the increasing of As(III)/Sb(III) ratio, so mixed crystal region is observed in the As(III)/Sb(III) ratio range of 0.82−1.22. Under the conditions of high As(III)/Sb(III) ratio, i.e. >1.5, the obtained deposits are fully amorphous and the As content is not less than 38.42 wt.%. In addition, it is noticed that the surface of crystalline-state deposits

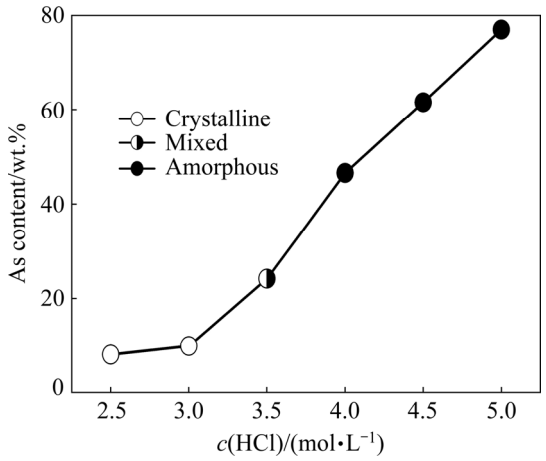

Fig. 7 Effects of HCl concentration on As content and structure form of deposits prepared from solutions containing 1.0 g/L As(III) and 4.0 g/L Sb(III)

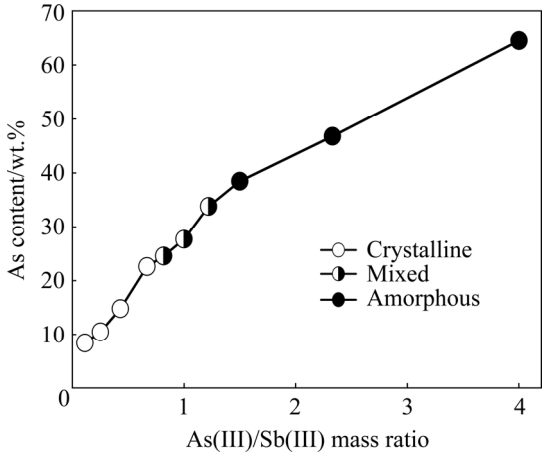

Fig. 8 As content and crystal structure evolution of deposits derived from solutions with 3.0 mol/L HCl and different As(III)/Sb(III) mass ratios (Total amount of As(III) and Sb(III): 5.0 g/L)

becomes rough and crystal structure becomes loose with the increased As(III)/Sb(III) ratio, and as a result, the appearance changes from typical metallic luster to black. However, for the amorphous deposits, their surfaces are flat, slippery and compact. The above results suggest that As content of the deposits increases with the increasing of As(III)/Sb(III) ratio in electrolyte, and the structure changes from crystalline to amorphous accordingly.

3.3 Effects of temperature on AsSb electrodeposition

Figure 9 shows the As content and crystal structure evolution of the deposits prepared at different temperatures. It is observed from Figs. 9(a, b) that the temperature can change the product structure while has little effect on the As content. When the temperature is 10 °C, amorphous deposits with about 10 wt.% of arsenic are obtained from the solution containing 3.0 mol/L HCl, 1.0 g/L As(III) and 4.0 g/L Sb(III). For the case of 15 °C, the deposits have mixed structure and crystalline deposits can only be obtained at higher temperatures.

Figures 9(c, d) present much detailed description on how temperature influences the product structure. By comparison, it is clear that the low electrolysis temperature is beneficial to the formation of amorphous deposits, while higher temperature will improve the formation of crystalline deposits. Specifically, in the case of 20 °C, to get amorphous deposits, we must keep the As(III) concentration not below 3.0 g/L. However, as the temperature drops to 15 °C, amorphous deposits can be obtained at 1.25 g/L As(III), which is far below that under 20 °C.

Figure 10 shows the micro-morphology of deposits prepared at different temperatures. It can be seen that the microscopic surface of deposits is relatively smooth and compact when the temperature is 10 °C. No crystal grains are observed on the nodular unit cells, i.e. amorphous structure as identified by XRD analysis. For the sample prepared at 30 °C, a rough surface with lots of octahedral particles is observed.

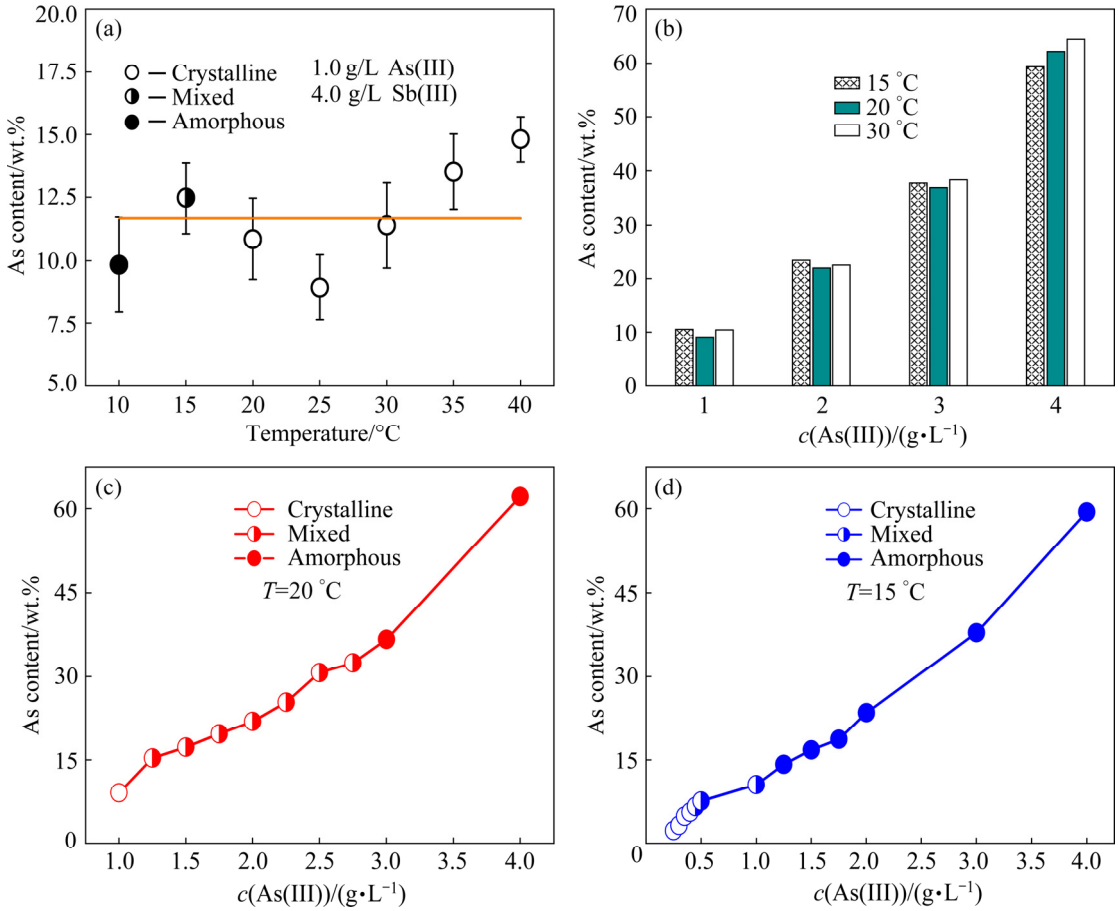

Fig. 9 Effects of temperature on As content and structure form of deposits obtained from solutions containing 3.0 mol/L HCl and 5.0 g/L As(III)+Sb(III)

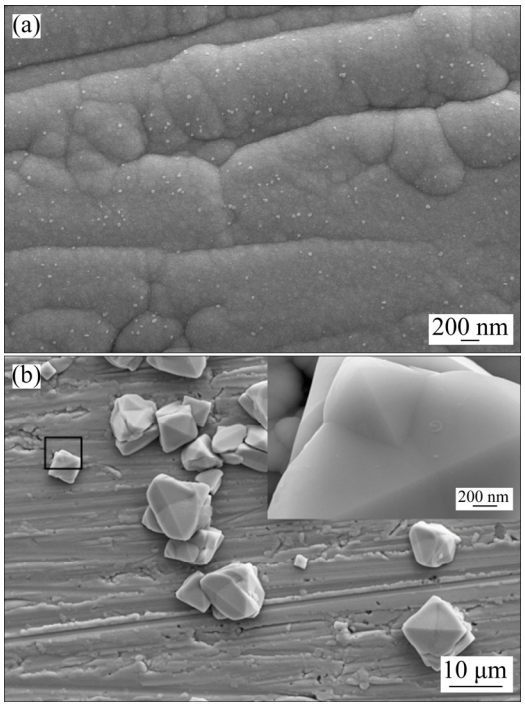

Fig. 10 Micro-morphologies of deposits prepared for 200 s from solutions containing 1.0 g/L As(III), 4.0 g/L Sb(III) and 3.0 mol/L HCl at different temperatures: (a) 10 °C; (b) 30 °C

4 Conclusions

(1) AsSb alloy with different As contents (0.70−95.81 wt.%) and phase structure can be directly fabricated by electrodeposition in As(III)−Sb(III)−HCl system. The phase structure of AsSb alloy evolves from crystalline to amorphous with the increasing of As content.

(2) Hydrochloric acid plays an important role in regulating the composition of electrodeposition products. According to thermodynamic analysis, the increase of acidity causes the reduction potential of As(III) to shift positively, while the adding of Cl^- increases the overpotential of Sb(III) reduction, which ultimately results in the significant increase of As content with increasing the HCl concentration.

(3) The electrolysis temperature has little influence on the composition of products, but the phase structure evolves from crystalline to amorphous with the decreasing of temperature.

(4) This study provides a special way to prepare AsSb alloy with different compositions and phase structures, which could be used for different purposes.

Acknowledgments

The authors are grateful for the financial supports from the National Natural Science Foundation of China (No. 51374185).

References

[1] XIAO Jun, WANG Ling-qing, DENG Li, JIN Zhang-dong. Characteristics, sources, water quality and health risk assessment of trace elements in river water and well water in the Chinese Loess Plateau [J]. Science of the Total Environment, 2019, 650(2): 2004−2012.

[2] RAVINDRA K, MOR S. Distribution and health risk assessment of arsenic and selected heavy metals in Groundwater of Chandigarh, India [J]. Environmental Pollution, 2019, 250: 820−830.

[3] LI Zhang-tao, WANG Lu, MENG Jun, LIU Xing-mei, XU Jian-ming, WANG Fan, BROOKES P. Zeolite-supported nanoscale zero-valent iron: New findings on simultaneous adsorption of Cd(II), Pb(II), and As(III) in aqueous solution and soil [J]. Journal of Hazardous materials, 2018, 344(15): 1−11.

[4] MIN Xiao-bo, LIAO Ying-ping, CHAI Li-yuan, YANG Zhi-hui, XIONG Shan, LIU Lin, LI Qing-zhu. Removal and stabilization of arsenic from anode slime by forming crystal scorodite [J]. Transactions of Nonferrous Metals Society of China, 2015, 25(4): 1298−1306.

[5] HU Bin, YANG Tian-zu, LIU Wei-feng, ZHANG Du-chao, CHEN Lin. Removal of arsenic from acid wastewater via sulfide precipitation and its hydrothermal mineralization stabilization [J]. Transactions of Nonferrous Metals Society of China, 2019, 29(11): 2411−2421.

[6] HE Xing-yu, DENG Fang, SHEN Ting-ting, YANG Li-ming, CHEN De-zhi, LUO Jian-feng, LUO Xu-biao, MIN Xiao-ye, WANG Fang. Exceptional adsorption of arsenic by zirconium metal−organic frameworks: Engineering exploration and mechanism insight [J]. Journal of Colloid and Interface Science, 2019, 539(15): 223−234.

[7] KUMAR M, RAO T S, ISLOOR A M, IBRAHIM G P S, INAMUDDIN, ISMAIL N, ISMAIL A F, ASIRI A M. Use of cellulose acetate/polyphenylsulfone derivatives to fabricate ultrafiltration hollow fiber membranes for the removal of arsenic from drinking water [J]. International Journal of Biological Macromolecules, 2019, 129(15): 715−727.

[8] KIM J, BENJAMIN M M. Modeling a novel ion exchange process for arsenic and nitrate removal [J]. Water Research, 2004, 38(8): 2053−2062.

[9] NIDHEESH P V, BABU D S, DASGUPTA B, BEHARA P, RAMASAMY B, KUMAR M S. Treatment of arsenite-contaminated water by electrochemical advanced oxidation processes [J]. Chemelectrochem, 2020, 7(11): 2418−2423.

[10] YANG Jin-qin, CHAI Li-yuan, LI Qing-zhu, SHU Yu-de. Redox behavior and chemical species of arsenic in acidic aqueous system [J]. Transactions of Nonferrous Metals Society of China, 2017, 27(9): 2063−2072.

[11] CAO Hua-zhen, SHU Yan-xiang, ZHANG Yu-feng, SHAN Hai-peng, ZHENG Guo-qu. Kinetics of cathodic reaction in

As(III) hydrochloric acid system [J]. The Chinese Journal of Nonferrous Metals, 2018, 28(12): 2551−2557. (in Chinese)

[12] WEI Z, SOMASUNDARAN P. Cyclic voltammetric study of arsenic reduction and oxidation in hydrochloric acid using a Pt RDE [J]. Journal of Applied Electrochemistry, 2004, 34(2): 241−244.

[13] BEJAN D, BUNCE N J. Electrochemical reduction of As(III) and As(V) in acidic and basic solutions [J]. Journal of Applied Electrochemistry, 2003, 33(6): 483−489.

[14] CAO Hua-zhen, ZHANG Yu-feng, WANG Qian-qian, WU Lian-kui, ZHENG Guo-qu. Nucleation/growth mechanism of electrocrystallization for As–Sb alloy in hydrochloric acid system [J]. Transactions of Nonferrous Metals Society of China, 2017, 27(10): 2291−2299.

[15] CAO Hua-zhen, ZHONG Yang, WU Lian-kui, ZHANG Yu-feng, ZHENG Guo-qu. Electrodeposition of As−Sb alloy from high arsenic-containing solutions [J]. Transactions of Nonferrous Metals Society of China, 2016, 26(1): 310−318.

[16] CAO Hua-zhen, SHAN Hai-peng, RUAN Hui-min, ZHENG Guo-qu. A study on the evolution of arsine during arsenic electrodeposition: The influence of ammonium citrate [J]. Electrochemistry Communications, 2012, 23(1): 44−47.

[17] SHAN Hai-peng, CAO Hua-zhen, ZHANG Yu-feng, RUAN Hui-min, ZHENG Guo-qu. Inhibitory effect of antimony on the evolution of arsine during electrochemical Co-deposition of arsenic with antimony [J]. Journal of the Electrochemical Society, 2013, 160(10): 121−124.

[18] SHU Yan-xiang, CAO Hua-zhen, WU Lian-kui, HOU Guang-ya, TANG Yi-ping, ZHENG Guo-qu. The comprehensive utilization of oxidative hydrochloric acid leaching of anode slime bearing fluorine, arsenic and antimony [J]. Hydrometallurgy, 2019, 183: 106−111.

[19] MUNTYANU F M, PYRTSAK K M, GLEVSKIL A. Giant quantum oscillations of the magnetothermoelectric coefficient in semimetallic Sb−Bi and Sb−As alloys [J]. Physics of the Solid State, 2001, 43(2): 214−217.

[20] MOISEEV K D, ROMANOV V V, VORONINA T I, LAGUNOVA T S, MIKHAILOVA M P, YAKOVLEV Y P. Type II $GaAs_xSb_{1-x}$/InAs (x<0.35) heterojunction grown by MOVPE near a miscibility gap of the ternary solid solution [J]. Journal of Crystal Growth, 2008, 310(23): 4846−4849.

[21] CRAIG A P, MARSHALL A R, TIAN Zhao-bing, KRISHNA S, KRIER A. Mid-infrared InAs0.79Sb0.21-based *nBn* photodetectors with Al0.9Ga0.2As0.1Sb0.9 barrier layers, and comparisons with InAs0.87Sb0.13 *p-i-n* diodes, both grown on GaAs using interfacial misfit arrays [J]. Applied Physics Letters, 2013, 103(25): 253502.

[22] JOSHI K B, PATEL N N, SWARNKAR C B, PALIWAL U. Electronic structure of $In_xGa_{1-x}As_ySb_{1-y}$ alloys [J]. Computational Materials Science, 2010, 49(4): 246−250.

[23] VURGAFTMAN I, MEYER J R, RAM-MOHAN L R. Band parameters for III−V compound semiconductors and their alloys [J]. Journal of Applied Physics, 2001, 89(11): 5815−5875.

[24] KABANAU D M, LEBIADOK Y V, YAKOVLEV Y P. Auger recombination and amplified luminescence in InAsSb/InAsSbP leds at 10−60 K [J]. Journal of Applied Spectroscopy, 2017, 84(5): 843−849.

[25] BOUNAB S, BENTABET A, BOUHADDA Y, BELGOUMRI G, FENINECHE N. First-principles calculations of structural, electronic and optical properties of ternary semiconductor alloys ZAs_xSb_{1-x} (Z=B, Al, Ga, In) [J]. Journal of Electronic Materials, 2017, 46(8): 4805−4814.

[26] HOMMA H, NAGATA H, YAMAGUCHI S. The effect of InAsSb buffer layer on the thermoelectric properties of MOCVD-grown InSb thin films [J]. ECS Transactions, 2010, 25(33): 87−96.

[27] MUNTYANU F M. Quantum oscillations of magneto-resistance and thermomagnetic power and the Fermi surface of As−Sb alloys [J]. Physica Status Solidi, 1986, 136(2): 749−756.

[28] SENANAYAKE G, MUIR D M. Speciation and reduction potentials of metal ions in concentrated chloride and sulfate solutions relevant to processing base metal sulfides [J]. Metallurgical & Materials Transactions B, 1988, 19(1): 37−45.

[29] DEAN J A. Lange's handbook of chemistry [M]. 2nd ed. Beijing: Science Press, 1999.

酸性氯化物体系中电沉积 AsSb 合金的组成与结构

舒燕翔，曹华珍，张惠斌，徐圣航，侯广亚，唐谊平，郑国渠

浙江工业大学 材料科学与工程学院，杭州 310014

摘　要：通过电沉积法在含 As(III)和 Sb(III)的盐酸溶液中制备 AsSb 合金(0.70%~95.81% As，质量分数)，并研究电解质成分、盐酸浓度和温度对 AsSb 合金组成和结构的影响。通过热力学分析 As(III)和 Sb(III)在盐酸溶液中的电还原机理。结果表明，H^+浓度的增加能促进 As(III)的还原，而 Cl^-浓度的增加则显著抑制 Sb(III)的还原，因此，沉积物中的 As 含量随电解液中 HCl 浓度的上升而逐渐增加，同时，产物的结构从晶态转变为非晶态。当 As 含量为 24.55%~33.75%(质量分数)，产物为 AsSb 晶态与非晶态的混合物。电解温度对沉积物的组成影响较小，但 AsSb 合金的结构随温度的降低从晶态转变为非晶态。

关键词：AsSb 合金；成分；物相；盐酸；热力学分析

(Edited by Bing YANG)